Feasibility study of a mm-wave impulse radio using measured radio channels

Haneda, Katsuyuki; Tufvesson, Fredrik; Wyne, Shurjeel; Ärlelid, Mats; Molisch, Andreas

Published in:
[Host publication title missing]

DOI:
10.1109/VETECS.2011.5956476

2011

Feasibility Study of a Mm-Wave Impulse Radio Using Measured Radio Channels

Katsuyuki Haneda[#], Fredrik Tufvesson[*], Shurjeel Wyne[†], Mats Ärlelid[*], and Andreas F. Molisch[‡]

[#] *Aalto University School of Electrical Engineering, SMARAD Centre of Excellence, Finland*
[#]Katsuyuki.Haneda@aalto.fi
[*] *Department of Electrical and Information Technology, Lund University, Sweden*
[†] *COMSATS Institute of Information Technology, Islamabad, Pakistan*
[‡] *Department of Electrical Engineering, University of Southern California, Los Angeles, CA, USA*

***Abstract*—A millimeter-wave (mm-wave) impulse radio is an attractive alternative to existing high-speed mm-wave radio systems because of the potential for a simpler transceiver architecture. This paper studies the feasibility of a mm-wave impulse radio system for home and office use by considering state-of-the-art transceivers and multiple-input multiple-output measured propagation channels as well as the IEEE 802.15.3c channel model. Our analysis reveals that reliable data transmission is infeasible even in line-of-sight (LOS) scenarios because of a low power level at the Rx if we do not use beamforming. However, introducing 7×7 beamforming at the Tx dramatically improves the coverage beyond 5 m distance in the LOS scenario and up to 5 m in a non-line-of-sight (NLOS) scenario, though the performance varies in the NLOS scenario, depending on the Tx and Rx locations. We propose an adaptive transmit signaling scheme that adjusts the pulse repetition frequency depending on the delay dispersion of the propagation channel in order to avoid intersymbol interference and keep the Rx structure simple. The proposed transmit signaling scheme leads to a pulse transmission rate of 250 Mpulses/s in all measured channels while the rate is lower when the 802.15.3c model is considered because of a more multipath-rich characteristics than our measured channels.**

I. Introduction

The scarcity of frequency resources and congestion of existing radio systems in the microwave band necessitates exploration of higher frequencies for high-data-rate radio systems. The millimeter-wave (mm-wave) band can meet the demand because of the availability of much wider bandwidths than in the microwave band. Furthermore, the mm-wave signals allow denser deployment of cells because of high free space attenuation, leading to less interference between cells and hence improved spectral efficiency per area unit. In order to realize the potential of mm-wave systems in practice, there are standardization activities of mm-wave radio systems for local and personal area networks [1], [2].

The mm-wave high-speed systems in the literature mostly consider orthogonal frequency division multiplexing (OFDM) or single-carrier (SC) transmissions as a physical layer technique [3]. OFDM provides scalable data rates but the transceiver complexity is fairly high; a fast Fourier transform at a clock rate up to several Gsamples leads to high power consumption. Furthermore, high peak-to-average ratio of radio signals hinders power efficient operation of amplifiers. On the other hand, with SC transmission the intention is to realize mm-wave radio systems with lower transceiver complexity and power consumption. Still, the receivers need high-resolution A/D converters and equalizers.

As an alternative to the OFDM and SC transmissions, this paper considers impulse radio. An impulse radio transmitter (Tx) creates a pulse directly by triggering an impulse generator. At the receiver (Rx), only a diode detector is required, therefore the need for signal processing is significantly reduced. It is also an advantage of the impulse radio receiver that it can work with a low-resolution A/D converter. The impulse radio transceiver development has been considered mainly in the low-frequency ultrawideband systems (below 10.6 GHz), *e.g.,* [4], [5] and references therein. However, thanks to the progress of semiconductor technology, development of the impulse radio transceiver has also been performed in the mm-wave range [6], [7].

In this paper we aim to investigate the feasibility of mm-wave impulse radio for home and office use such as sending video files from a DVD player to a display, or from a laptop to a projector. To this end, it is of fundamental importance to investigate the mm-wave radio channel in which the impulse radio will operate. The mm-wave propagation differs from that of conventional low-frequency radios both in pathloss and delay dispersion characteristics; the free space loss, reflection, diffraction, and scattering losses are larger than those at lower frequencies. Consequently, system coverage becomes smaller and a lower delay spread is typically observed [8]. Since it is not always straightforward to increase transmit power of millimeter-wave signals using amplifiers, high gain antennas are installed at either, or both, link ends. Thanks to the wavelength of mm-wave radio, as small as 5 mm at 60 GHz, it is possible to implement multiple antennas or antennas having electrically large aperture size on a physically small RF front-end, *e.g.*, [9]. The multiple antennas give a possibility to perform beamforming in order to constructively add transmit and receive signals thereby increasing the equivalent isotropic radiated power (EIRP) and receive signal-to-noise ratio (SNR).

This work is based on the Tx and Rx schemes presented in [6], [7]. We first study the link-budget to estimate the range of communications that the mm-wave impulse radio can cover. We then perform a delay dispersion analysis to obtain maximum throughputs without considering error control coding. The effect of beamforming to improve the communication range and mitigate delay dispersion is also

978-1-4244-8331-0/11/$26.00 ©2011 IEEE

investigated. Two kinds of propagation channels are used for the analysis: a spatial channel model developed in the IEEE 802.15.3c [10] and multiple-input multiple-output (MIMO) channel measurements in office and meeting rooms, in order to observe differences of those two channels.

II. Mm-Wave Impulse Radio

The Tx we consider in this paper generates pulses having 100 ps width triggered directly by a baseband signal with pulse repetition frequency up to 12.5 GHz [6]. The power spectrum of the puluses shows that the transmit power is concentrated around 60 to 70 GHz. In this analysis we set the frequency range of interest to 61 to 65 GHz because it corresponds to the frequency range of the channel measurements. Integrated over the frequency range, the transmit power P_{t} was found to be -7 dBm. The mean SNR at the Rx γ is given by

$$\gamma = P_{\mathrm{t}}(PL \cdot P_{\mathrm{n}})^{-1}, \tag{1}$$

where P_{n} is the noise level at the Rx and PL denotes distance-dependent pathloss experienced by the radio waves which includes the Tx and Rx antenna gains. The antenna gains may include array gain due to beamforming. Impulse radios can employ one of several modulation formats, and in this paper, we consider on-off keying (OOK) and binary pulse position modulation (BPPM). Setting the target bit error rate (BER) to 10^{-6}, it is possible to identify the minimum SNR required at the Rx [11]; they are 13.5 and 14.1 dB for the OOK and BPPM.

According to [7], there is a tradeoff between the pulse sampling rate and sensitivity level at the Rx. In this paper we assume the Rx to operate at sampling rate of 250 Mpulses/s with $P_{\mathrm{n}} = -70$ dBm sensitivity. The pulse generation rate of the Tx is set to 250 Mpulses/s in order to be compatible with the sampling rate of the Rx. Furthermore, it is assumed that a sequence of transmit pulses can have a guard period between pulses in order to avoid intersymbol interference at the Rx at the expense the pulse repetition rate. The length of the guard period is determined such that all significant energy of the transmitted pulse, due to multipath propagation, arrives at the Rx before the next pulse is received. With this signaling arrangement, it is not necessary to implement an equalizer at the Rx, thus simplifying the Rx structure. A transmit symbol is therefore composed of a pulse of width T_{p} and guard period T_{b}, resulting in a pulse repetition rate of $(T_{\mathrm{p}} + T_{\mathrm{b}})^{-1}$. Let τ_{w} be the delay window of radio channel within which all significant multipaths arrive. If $\tau_{\mathrm{w}} \leq T_{\mathrm{p}}$ there is no need to insert the guard period, but otherwise a guard period of length $T_{\mathrm{b}} = \tau_{\mathrm{w}} - T_{\mathrm{p}}$ is needed. At the Rx, multipaths that arrive within the guard period can be collected by the Rake receiver to increase the receiving SNR [12]. It is therefore crucial to know τ_{w} in real-world radio propagation channels. Furthermore, the effect of beamforming on the improvement of the receiving SNR and reduction of delayed multipaths is also analyzed in a similar manner as [13]. Considering the feasibility of hardware implementation, let us use the beamforming only on the Tx side where a set of impulse generators attached to antennas are triggered by baseband signals at different time instants such that the generated pulses are constructively added at the Rx. With this configuration it is not necessary to introduce phase shifters in the radio frequency stage which would incur losses of the transmit power.

III. Radio Channel Models and Measurements

A. IEEE 802.15.3c Channel Model

The IEEE 802.15.3c channel model is a spatio-temporal model for mm-wave radio systems [10]. The channel model is based on the Saleh-Valenzuela model for the delay domain properties, while angular characteristics are included at one link end. The channel model supports several scenarios, for example, residential, office, and kiosk scenarios. Each scenario consists of line-of-sight (LOS) and non line-of-sight (NLOS) cases. In this analysis, office environments under both LOS (CM32) and NLOS (CM41) conditions are considered. The channel models were constructed by rotating a directional antennas having 60° and 15° 3-dB beamwidths in the LOS and NLOS conditions respectively, which determines the angular resolution of the channel models. Assuming the reciprocity of radio channels, let the Tx side have angular characteristics at which the beamforming is performed. Furthermore, we assume that the antenna elements at the Tx and Rx are the same as those used in the propagation measurements. This allows us to make a fair comparison between channel measurements and channel model outputs. The "golden sets" [10] of channel model outputs, which consist of 100 channel impulse responses, were obtained under the same specifications of the center frequency and bandwidth as those of the channel measurements, and used for the feasibility study. The channels were generated for the Tx-Rx distance of $1, 2, 3$, and 4 m.

B. Channel Measurements

1) Measurement Environments: The mm-wave channel measurements were performed in two rooms of a modern office building in Aalto University, Espoo, Finland; one in an office room and another in a meeting room with the volume of $4.3 \times 4.9 \times 2.8$ m^3 and $6.8 \times 7.0 \times 2.5$ m^3, respectively. During the measurements the Rx array remained fixed at one location of the room, while a channel measurement was performed by placing the Tx array at one of 64 and 17 predefined positions located on table tops as shown in Fig. 1. Both scenarios had a line-of-sight (LOS) between the Tx and Rx. In the meeting room, however, a non-line-of-sight (NLOS) scenario was also measured except at two positions shown in Fig. 1(b). The measured NLOS scenarios were created by blocking the first Fresnel-zone with a laptop screen. Most of the measurements were performed during night time when there were no other people in the building, and when measuring during the day the movement of people was prevented in the vicinity of the measurement area to maintain a time-static measurement environment.

2) Measurement Equipment: The channel transfer functions were measured with a vector network analyzer (VNA) based system [14]. The Tx power was set to $+7$ dBm, and the measured frequency range from 61 to 65 GHz was spanned by 1001 equidistantly-spaced frequency tones. At the Tx side a

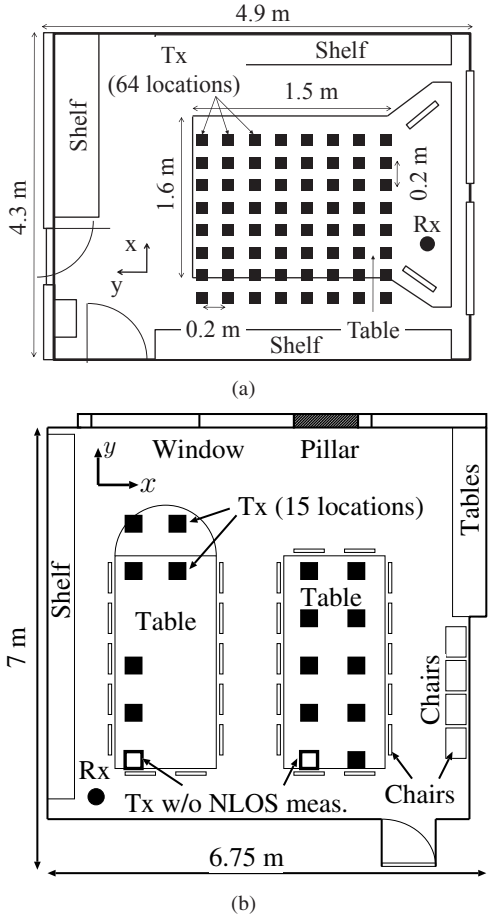

Fig. 1. Floor plans of the measurements in (a) an office room and (b) a meeting room.

7×7 virtual planar array was scanned on the horizontal plane using a 2-D electromechanical positioner. The Tx element was a vertically polarized commercial biconical antenna with an omnidirectional pattern in azimuth. At the Rx side a 7×7 virtual planar array was scanned on the vertical plane using another 2-D positioner. For the office room measurements, a biconical antenna, which is the same type as the Tx, was used as the Rx element, while in the meeting room a vertically polarized open waveguide was used. With these Tx and Rx array settings, we model a practical case of transmission from a DVD player or similar device, placed on the table, to a high-definition display device placed in the corner of the room. The virtual arrays at Tx and Rx had an inter-element spacing of 2 mm such that the length of one side of the 7×7 planar array was 12 mm. The Tx antenna when placed on the table surface, had a height of 1.1 m above the floor. Thanks to the virtual arrays, the transfer functions for $49 \times 49 = 2401$ channel combinations were recorded at each Tx and Rx position. The measurement SNR was in the range of 40 to 68 dB where the worst case SNR values were observed in the NLOS scenarios of the meeting room at the largest Tx-Rx separations. Prior to measurements the equipment was back-to-back calibrated; the response of the VNA, frequency-converters, cables, connectors, and waveguides were then removed from the measured frequency responses in a post-processing step, before the analysis.

IV. Effects of Beamforming

In order to characterize the effect of beamforming on the link budget and transmit signaling, this section defines the pathloss, PL, and the delay window, τ_{w} based on the channel model outputs and measured channels.

A. Beamforming for the 802.15.3c Channel Model Outputs

The output of the 802.15.3c model is an impulse response h_{cm} which consists of a set of discrete propagation paths spread over the delay and angular domains as

$$h_{\mathrm{CM}} = \sum_{l} \alpha_l \delta(\phi - \phi_l)\delta(\tau - \tau_l), \tag{2}$$

where α_l, ϕ_l, τ_l are the complex amplitude, azimuth angle, and delay time of the l-th path; (2) implies that the path parameters are constant over the frequency of interest from 61 to 65 GHz in our case. This assumption is reasonable since relative bandwidth is as small as 6 %. The beamforming finds the strongest path having an angle ϕ_{peak} and delay τ_{peak}, and then the array gain to that path. The channel impulse response after the beamforming is given by

$$h_{\mathrm{CM,BF}} = \sum_{l} \alpha_l \delta(\phi - \phi_l)\delta(\tau - \tau_l)\sqrt{G_{\mathrm{Tx}} G_{\mathrm{Rx}} \mathbf{a}^H(\phi_l)\mathbf{a}(\phi_{\mathrm{peak}})}, \tag{3}$$

where $\mathbf{a}(\phi) \in \mathbb{C}^{N_{\mathrm{Tx}}}$ is an array steering vector, G_{Tx} and G_{Rx} are the gain of Tx and Rx antenna elements, respectively, and $\cdot^H$ denotes the Hermitian conjugate of a matrix. According to an antenna pattern measurement [15], the antenna gain is set to a constant value of 1.8 dBi and 8.5 dBi for the biconical antenna and open waveguide, respectively. This setting is valid since we assume that the broadside of the Tx antenna always points to the Rx. The n-th row of the array steering vector is given by

$$a_n(\phi) = \exp\left\{-\mathrm{j}2\pi\lambda^{-1}\langle \mathbf{u}(\phi), \mathbf{d}_n \rangle\right\}, \tag{4}$$

where λ is the wavelength at the center frequency of the system, $\mathbf{u}(\phi) = [\cos\phi \quad \sin\phi \quad 0]^T$ is a unit directional vector for the azimuth angle of interests, $\mathbf{d}_n = [d_x \quad d_y \quad d_z]^T$ is a position vector of the n-th antenna element relative to the array center, $\langle \mathbf{x}, \mathbf{y} \rangle$ is an inner product of two vectors $\mathbf{x}$ and $\mathbf{y}$, and $\cdot^T$ is a transpose operation.

B. Beamforming for Measured Channel Data

Since our analysis considers beamforming only on the Tx side, it is sufficient to use only a single antenna element in the Rx array; in our case, the center element was chosen. Therefore each MIMO channel is reduced to a multiple-input-single-output (MISO) channel containing 49 channel transfer functions. The MISO channel is denoted in a matrix form as $\mathbf{H} \in \mathbb{C}^{N_{\mathrm{Tx}} \times N_{\mathrm{f}}}$ where $N_{\mathrm{Tx}} = 49$ and $N_{\mathrm{f}} = 1001$ are number of antenna elements in the Tx array and frequency samples.

In order to perform the beamforming for the strongest paths, it first is necessary to know $\phi_{\rm peak}$ and $\tau_{\rm peak}$ by

$$(\phi_{\rm peak}, \tau_{\rm peak}) = \arg\max_{\phi,\tau} \left\{ \mathrm{vec}\left(\mathbf{W}(\phi,\tau)\right)^H \mathrm{vec}\left(\mathbf{H}\right) \right\}, \quad (5)$$

where $\mathrm{vec}(\cdot)$ denotes matrix vectorization and $\mathbf{W}$ is a weight matrix whose entries are

$$W_{n,m}(\phi,\tau) = \exp\left\{ -\mathrm{j}2\pi f_m \left(\tau + \frac{\langle \mathbf{u}(\phi), \mathbf{d}_n \rangle}{c} \right) \right\}. \quad (6)$$

In (6) f_m is the frequency corresponding to the m-th frequency bin and c denotes the velocity of light. The channel impulse response after the beamforming for the strongest path is then given by

$$h_{\rm MS,BF}(\tau) = \mathrm{vec}\left(\mathbf{W}(\phi_{\rm peak}, \tau_{\rm peak})\right)^H \mathrm{vec}\left(\mathbf{H}\right). \quad (7)$$

C. Pathloss and Delay Window

Let us assume that the Rx detects a peak of the incoming signal for demodulation. This simple Rx structure corresponds to a selective Rake receiver having only a single finger [12]. Hence the pathloss in this study is defined by the peak level of the impulse response. For a given channel impulse response, the pathloss is calculated by

$$PL = \left\{ \max\left(|h(\tau)|^2 \right) \right\}^{-1}. \quad (8)$$

Substituting (8) into (1) yields the SNR at the Rx. The delay window is defined by [11]

$$\tau_{\rm w} = \arg\min_{\tau} \left\{ \int_{\tau_0}^{\tau_0+\tau} |h(x)|^2 \mathrm{d}x > \frac{\eta P}{1+\eta} \right\}, \quad (9)$$

where $P = \int_0^\infty |h(x)|^2 \mathrm{d}x$ is the total power of the channel impulse response and the threshold value, η, is set to 10 dB. For a given channel impulse response, $\tau_{\rm w}$ gives the shortest delay interval such that the power within the interval is η dB higher than the power outside the interval. This definition is intended to give a quantitative measure of the self-interference caused by the delay dispersion of channels.

V. Results and Discussions

A. SNR at the Rx

Figure 2 shows the SNR against Tx-Rx distance in an office and a meeting room. Each plot consists of results without beamforming, *i.e.,* a single element Tx and Rx, and those with beamforming at the Tx by the 7×7 horizontal uniform rectangular array. The results from the office contain only LOS channels while LOS and NLOS channels are shown separately for the meeting room. The SNR derived from the LOS and NLOS channel of the 802.15.3c model is also plotted for comparison. Since the 802.15.3c model output consists of 100 channel realizations for each Tx-Rx distance, only the median value is shown on the plot. The results show close agreement between the channel measurements and 802.15.3c model, hence the pathloss model used in the 802.15.3c model was found to be applicable in our measurement scenario. However, a strange behavior of the pathloss was found in the NLOS 802.15.3c model; the SNR at the Rx increased as the Tx-Rx distance became larger. Another important finding is that the SNR is fairly low when beamforming is not used, and is generally not fulfilling the required SNR for the OOK and BPPM as discussed in Section II even in the LOS conditions. However, the SNR is sufficiently high in LOS scenarios with beamforming, making it possible to use OOK and BPPM up to 5 m Tx-Rx distances in the LOS scenarios. The beamforming also increases the receiving SNR to about 15 dB when installed in the NLOS condition, but fluctuation of the SNR level is within a ± 10 dB range, which would incur unstable performance depending on Tx locations.

B. Delay Window

Delay windows of the three scenarios are shown in Fig. 3. The plots from the 802.15.3c model show the median value of the 100 channel realizations. Each figure contains results with and without beamforming. The results show that the delay window is 0 ns in all the measured channels even without beamforming, while that of the 802.15.3c model gives non-zero values without beamforming. The delay window was not necessarily reduced to zero even when the beamforming was introduced and was as large as 120 ns in the NLOS channels. This indicates that the 802.15.3c model gives more multipath-rich environment than our measured channels. Therefore system evaluation with the 802.15.3c model could lead to a pessimistic result compared to a case with our channel measurement data. In our system of interests, the pulse width, $T_{\rm p}$, is 4 ns since the maximum pulse transmission rate is 250 Mpulses/s as discussed in Section II. When the measured channels are considered, there is no need to insert guard periods between adjacent pulses because $\tau_{\rm w} < T_{\rm s}$ holds, hence the maximum pulse transmission rate is achievable if the receiving SNR is sufficiently high. On the other hand, the guard period needs to be inserted when the 802.15.3c model is considered since $\tau_{\rm w} > T_{\rm s}$ in most cases. Having set the delay window to the symbol length, the pulse transmission rate becomes $1/\tau_{\rm w} \sim 12.8$ Mpulses/s at 1 m Tx-Rx distance in the LOS office scenario without beamforming, and 8.3 Mpulses/s in the NLOS meeting room with beamforming.

VI. Conclusion

A feasibility study of mm-wave impulse radio based on the state-of-the-art Tx and Rx was performed using the measured channels as well as the IEEE 802.15.3c channel model. The study revealed that the use of beamforming is crucial in ensuring sufficient coverage by the system; without beamforming, reliable data transmission is impossible both in LOS and NLOS scenarios. Using beamforming with a 7×7 antenna array, it is possible to extend the reliable communication range beyond 5 m in LOS scenarios, and up to 5 m in NLOS conditions. Still in NLOS scenarios the fluctuation of the SNR is within ± 10 dB range, making the operation unstable depending on channel conditions. We proposed an adaptive signaling scheme that adjusts the pulse repetition frequency to the delay window of propagation channels where most of energy falls into. This signaling avoids intersymbol interference at the Rx and thereby simplifies the Rx structure.

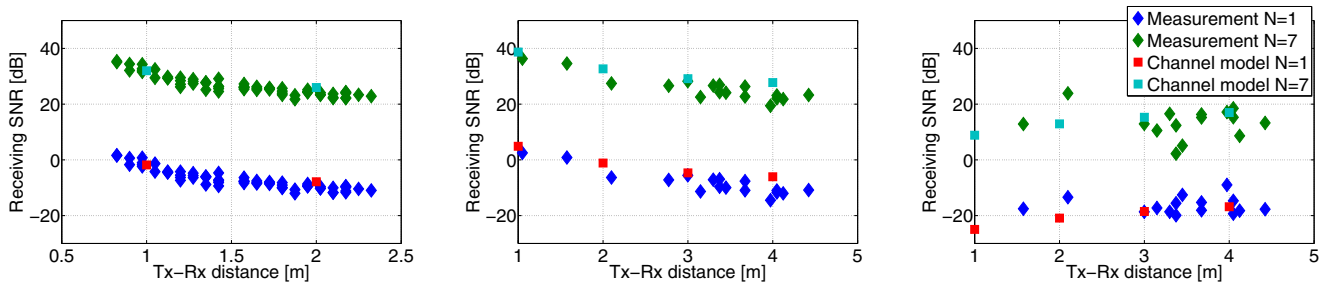

(a) (b) (c)

Fig. 2. Receiving SNR derived from channel measurements and the channel model for (a) LOS office, (b) LOS meeting room, and (c) NLOS meeting room scenarios.

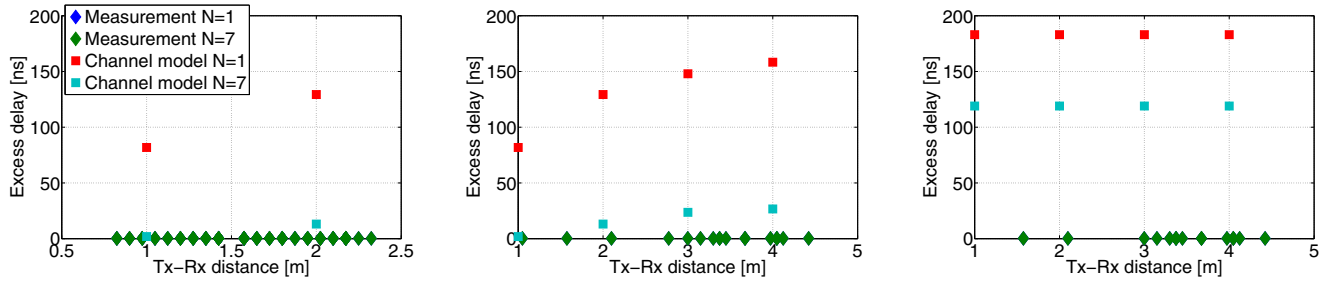

(a) (b) (c)

Fig. 3. Delay window derived from channel measurements and the channel model for (a) LOS office, (b) LOS meeting room, and (c) NLOS meeting room scenarios. Notice that the delay window was close to zero regardless of the use of beamforming in the measured channels, hence the two types of lozenges are totally overlapping in the figure.

With this signaling, it was found that pulse transmission with the maximum possible rate, 250 Mpulses/s, is feasible both in LOS and NLOS measured channels because of very small delay window. On the other hand, the pulse repetition frequency needs to be decreased when the 802.15.3c model is considered because of more multipath rich characteristics than our measured channels, leading to a more pessimistic system performance prediction.

ACKNOWLEDGMENT

K. Haneda would like to acknowledge the financial support of the post-doctoral research project of the Academy of Finland, Helsinki, Finland. This work was also partly supported by the Swedish Foundation for Strategic Research, the High Speed Wireless Center at Lund University, and a grant from Vetenskapsrådet, the Swedish Science Council.

REFERENCES

[1] IEEE P802.11 Task Group ad, http://www.ieee802.org/11/Reports/tgad_update.htm.

[2] IEEE Std 802.15.3c-2009, Oct. 2009.

[3] C. H. Park and T. S. Rappaport, "Short-range wireless communications for next-generation networks: UWB, 60 GHz millimeter wave PAN, and Zigbee," *IEEE Wireless Commun. Mag.*, vol. 14, no. 4, pp. 70–78, Aug. 2007.

[4] M. Anis, R. Tielert. N. Wehn, "3.1-to-7GHz UWB impulse radio transceiver front-end based on statistical correlation technique," in *Proc. Int. Symp. Cir. Sys. 2008 (ISCAS 2008)*, pp. 664–667, Seattle, WA, May 2008.

[5] A. Gerosa, S. Solda, A. Bevilacqua, D. Vogrig, and A. Neviani, "An energy-detector for noncoherent impulse-radio UWB receivers," *IEEE Trans. Cir. Sys. I*, vol. 56, no. 5, pp. 1030–1040, May 2009.

[6] M. Ärlelid, L. E. Wernersson, M. Egard, and E. Lind, "60 GHz ultra-wideband impulse radio transmitter," in *Proc. 2009 IEEE Int. Conf. Ultrawideband (ICUWB2009)*, pp. 185–188, Vancouver, Canada, Sep. 2009.

[7] M. Ärlelid, L. E. Wernersson, M. Egard, and E. Lind, "A 60 GHz super-regenerative oscillator for implementation in an impulse radio receiver," in *Proc. 2010 Int. Conf. Ultrawideband (ICUWB2010)*, Nanjing, China, Sep. 2010.

[8] C. R. Andersen and T. S. Rappaport, "In-building wideband partition loss measurements at 2.5 and 60 GHz," *IEEE Trans. Wireless Commun.*, vol. 3, no. 3, pp. 922–928, May 2004.

[9] W. F. Moulder, W. Khalil, and J. L. Volakis, "60-GHz two-dimensionally scanning array employing wideband planar switched beam network," *IEEE Ant. Wireless Prop. Lett.*, vol. 9, pp. 818–821, 2010.

[10] S.-K. Yong *et al.*, "TG3c channel modeling sub-committee final report," IEEE Tech. Rep., 15-07-0584-01-003c, Mar. 2007.

[11] A. F. Molisch, *Wireless Communications, Chapter 12 Demodulation*, John & Wiley and Sons, Chichester, UK, 2005.

[12] D. Cassioli, M. Z. Win, F. Vatalaro, and A. F. Molisch, "Low complexity rake receivers in ultra-wideband channels," *IEEE Trans. Wireless Commun.*, vol. 6, no. 4, pp. 1265–1275, Apr. 2007.

[13] S. Wyne, K. Haneda, S. Ranvier, F. Tufvesson, and A.F. Molisch, "Beamforming effects on measured mm-wave channel characteristics," *IEEE Trans. Wireless Commun.*, submitted.

[14] S. Ranvier, M. Kyro, K. Haneda, C. Icheln, and P. Vainikainen, "VNA-based wideband 60 GHz MIMO channel sounder with 3-D arrays," in *Proc. Radio Wireless Symp. 2009 (RWS2009)*, pp. 308–311, San Diego, CA, Jan. 2009.

[15] J. Simola, "Millimeter wave propagation measurements and modeling in hospital environments," Master Thesis of Aalto University School of Science and Technology, Department of Radio Science and Engineering, May 2010.